UDC 536.2.004.414.23:533.6.004.414.23 DOI: 10.18698/1812-3368-2021-2-102-117

NUMERICAL INVESTIGATION OF THERMAL-HYDRAULIC PERFORMANCE OF CIRCULAR AND NON-CIRCULAR TUBES IN CROSS-FLOW

R. Deeb[1] e.rawad.deeb@yandex.com
D.V. Sidenkov[1] sidenkovdv@mpei.ru
V.I. Salokhin[2] v.salohin@yandex.ru

[1] **National Research University Moscow Power Engineering Institute, Moscow, Russian Federation**
[2] **Russian Institute for Scientific and Technical Information, Moscow, Russian Federation**

Abstract

A numerical study has been conducted to clarify flow and heat transfer characteristics around circular, cam, and drop-shaped tubes using the software package *ANSYS FLUENT*. Reynolds number Re based on equivalent circular tube is varied in range of $(8.1–19.2) \cdot 10^3$. All tube shapes are investigated under similar operating conditions. Local heat transfer, pressure and friction coefficients over a surface of the tubes were presented. Obtained results agree well with those available in the literature. Correlations of the average Nusselt number Nu_{av} and a friction factor f in terms of Reynolds number for the studied tubes were proposed. The results indicated that Nu_{av} increases with increasing Re. In the contrary, f decreases as Re increases. Thermal-hydraulic performance η is used to estimate the efficiency of the cam and drop-shaped tubes. Results show that the drop-shaped tube has the best thermal-hydraulic performance, which is about 1.6 and 2.5 times higher than that of the cam-shaped and circular tube, respectively

Keywords

Circular tube, cam-shaped, drop-shaped, heat transfer, drop pressure, friction factor, thermal-hydraulic performance, numerical investigation

Received 13.07.2020
Accepted 12.01.2021

Introduction. Circular tubes bundles are widely used in heat exchange equipment because of the ease of production and its capability of withstanding a high pressure. In contrast to the circular tubes which cause severe separation and a large vortex zone to produce high pressure drops, non-circular tubes of streamlined shapes offer very low hydraulic resistance. Žukauskas and Ulinskas [1, 2] suggested correlations for heat transfer and pressure drop for staggered and in-

line of circular tubes bundles. The Reynolds number was in the range of 1 to $2 \cdot 10^6$, as well as a wide range of relative longitudinal and transverse spacing. They suggested an efficiency factor for the evaluation of heat transfer surfaces efficiency to improve heat exchangers constructions. Mittal et al. [3] numerically investigated the flows past a pair of cylinders in staggered and in-line arrangements for different longitudinal spacing using a stabilized finite element method. They concluded that with increasing the longitudinal spacing, the flow at Re = 100 showed unsteady behavior. Numerical simulation is carried out by Roychowdhury et al. [4] to investigate the effect of spacing on flow and heat transfer over staggered tube bundles. They observed that both the Reynolds number and tube spacing influence the vortex formation. As the tube spacing increases, the size and length of eddies increase. For sufficiently small spacing and for all values of Reynolds number, eddy completely suppressed. Nishiyama et al. [5] studied the effects of longitudinal spacing on the drag coefficient for the staggered tubes bundle. They concluded that to achieve compactness of the system and minimize the drag coefficient, the longitudinal spacing should be arranged as small as possible.

In recent years, cross-flow heat exchangers with non-circular tubes have attracted attention of many researchers. Lavasani [6] experimentally investigated the flow around cam shaped tube bank with inline arrangement for both longitudinal pitch ratios 1.5 and 2.0. It was noted that by increasing longitudinal pitch ratios from 1.5 to 2.0, heat transfer increases about 7–14 %. Furthermore, friction factor of cam shaped tube bank is approximately 95 % lower than circular tube bank. Merker and Hanke [7] experimentally investigated heat transfer and pressure drop of the cross-flow on the shell-side of staggered oval-shaped tubes bundle, having different transversal and longitudinal pitches. They found that the pressure drop decreases with increasing relative transversal pitch and Reynolds number. Horvat et al. [8] numerically compared the heat transfer conditions for the tube bundle in cross flow for different tube shapes as cylindrical, ellipsoidal, and wing-shaped. The pitch to the diameter ratio in the staggered arrangement was from 1.125 to 2.0. Their results showed that drag coefficient is lower for ellipsoidal and wing-shaped tubes than that for the cylindrical tubes. However, drag coefficient decrease with increasing the Reynolds number. Terekh et al. [9] experimentally investigated the aerodynamic drag of single drop-shaped and circular tubes in the narrow channel at the Reynolds number ranging from 9 000 to 45 000. The obtained data indicate a significantly lower aerodynamic drag of drop-shaped tubes compared to a circular one. The effects of angles of attack on the heat transfer characteristics and the drag coefficient for staggered drop-shaped tubes were experimentally and numerically investi-

gated by Sayed Ahmed et al. [10, 11]. They found that the average Nu values at zero angle of attack (θ = 0) was higher by about 76 % compared to elliptical tubes bundle with the same heat transfer surface. In addition, the lowest values of pressure drop were achieved at zero angle for all values of Reynolds numbers. Deeb and Sidenkov [12, 13] numerically studied hydrodynamics and heat transfer characteristics of a drop-shaped tubes bundle of various configurations. Their results indicate that the hydrodynamic resistance of the drop-shaped tubes bundles was better than the circular ones at angles of attack of 0, 180°. They proposed a correlation for heat transfer in terms of Re and θ with taking into account the stress-strain state of the tubes.

Computational Fluid Dynamics (CFD) emerged as a reliable and cost-effective method to simulate complex turbulent flows. Several researchers have identified the best combination of modeling and numerical method, in terms of accuracy and computational cost. Jafari and Dehkordi [14] numerically simulated the 2D unsteady viscous flow around two circular cylinders in a tandem arrangement in order to study the characteristics of the flow. Their results indicate that the extended k–ε and the Re-Normalization Group (RNG) k–ε models offer more accurate results than the standard k–ε model. Priyank et al. [15] used *FLUENT* Software to analyze for predicting fluid flow and heat transfer characteristics over a staggered tube bundle heat exchanger with different tube bundles. They reported that CFD is the best tool for predicting fluid flow and heat transfer characteristics prior to the physical setup of the experiments. RNG k–ε turbulence model improves the ability to model highly strained flows, vortices, separation, and recirculation of the fluid. The RNG k–ε model showed an excellent agreement between numerical and experimental results [16–18].

In the above-mentioned works, the local heat transfer and flow characteristics of the cam and drop-shaped tubes are not fully described, but only the overall heat transfer characteristics were presented. Thus, the details of the heat transfer and flow on the tube surface could not be discussed. The local heat transfer and hydrodynamic characteristics are particularly important in understanding the performance of tubes bundle.

In this regard, the subject of this study is to gain insight into the characteristics of local and average heat transfer and fluid flow around circular, cam, and drop-shaped tubes. Numerical simulation has been conducted using the software package *ANSYS FLUENT* to provide a detailed study of heat transfer, friction factor affecting the overall thermal performance of each tube. Correlations of the Nu_{av} and f for the studied tubes were obtained for $8.1 \cdot 10^3 \le \mathrm{Re}_{D\max} \le 19.2 \cdot 10^3$.

Numerical investigation. *Geometrical model.* In this study, three types of tubes have been investigated. Figure 1 shows the cross-sections of the circular,

cam, and drop-shaped tube. Tubes are located in a square cross-section channel; a side of the square cross-section is 305 mm (length × width = 780 × 305 mm). To compare the heat transfer and friction factor from each tube, the characteristic length D_{eq} = 22.44 mm is defined as the diameter of an equivalent circular tube.

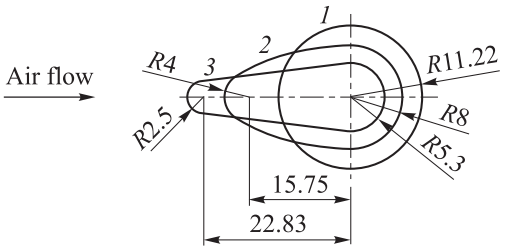

Fig. 1. Cross-sections of a circular (*1*); cam-shaped (*2*); drop-shaped tube (*3*)

Problem description and boundary conditions. The forced convection problem has been solved using *ANSYS FLUENT* [19] in a two-dimensional stationary formulation assuming a viscous incompressible flow with constant thermophysical properties, taking into account the possibility of turbulence generation. The effect of heat exchange by radiation are neglected. The numerical solution is carried out by solving the governing equations of mass, momentum, and energy:

$$\frac{\partial u}{\partial x}+\frac{\partial v}{\partial y}=0;$$

$$u\frac{\partial u}{\partial x}+v\frac{\partial u}{\partial y}=-\frac{1}{\rho}\frac{\partial p}{\partial x}+\nu\left(\frac{\partial^2 u}{\partial x^2}+\frac{\partial^2 u}{\partial y^2}\right);$$

$$u\frac{\partial v}{\partial x}+v\frac{\partial v}{\partial y}=-\frac{1}{\rho}\frac{\partial p}{\partial y}+\nu\left(\frac{\partial^2 v}{\partial x^2}+\frac{\partial^2 v}{\partial y^2}\right);$$

$$u\frac{\partial T}{\partial x}+v\frac{\partial T}{\partial y}=a\left(\frac{\partial^2 T}{\partial x^2}+\frac{\partial^2 T}{\partial y^2}\right),$$

where u is the x-component of the air velocity; v is the y-component of the air velocity; ρ is the air density; p is air pressure; ν is the air kinematic viscosity; a is thermal diffusivity; T is temperature of the liquid.

The turbulence is modeled by the two-equation of Re-Normalization Group (RNG) k–ε model with the "Enhanced wall Treatment" function [16, 19].

Reynolds number was calculated by $\mathrm{Re}_{D\max}=\rho U_{\max}D_{eq}/\mu$, where μ is a dynamic viscosity; $U_{\max}$ is the maximum velocity in the minimum free cross-section.

As an external flow, the air flow is used. All computational experiments were performed with a tube surface temperature of about 82.85 °C. The initial velocity of the air at the channel's entrance region varied in range of 6–12 m/s, which corresponds to $\mathrm{Re}_{D\max} = (8.1–19.2) \cdot 10^3$, at a temperature of 26.85 °C and atmospheric pressure.

Mesh generation. The mesh is generated using ICEM CFD. Figure 2 shows the configuration of the computational domain mesh for all studied tubes. The working fluid domain is meshed with quadrilateral mesh elements with refining the mesh near walls, so as to capture the boundary layer over the tube surface. The location of the first node away from a wall were kept at $1 < y^+ < 5$. The mesh quality of 0.926 is maintained for the entire simulation.

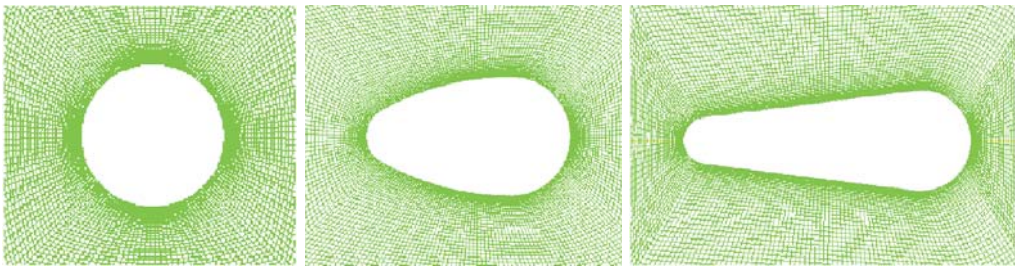

a *b* *c*

Fig. 2. Mesh details around the surface of the circular (*a*); cam-shaped (*b*); drop-shaped tube (*c*)

In this study, a finite-volume discretization method using second order upwind scheme for momentum, turbulent kinetic energy, and turbulent dissipation rate was performed. The simulation used the segregated solver, with which continuity and momentum equations were solved in a decoupled fashion during the outer iteration loop, besides using *SIMPLE* pressure-based solution algorithm of the velocity–pressure coupling. The solution was considered converged when the scaled residual of the energy and other equations reach 10^{-10}.

The mesh-sensitivity analysis was carried out mainly to check for a mesh independent solution. The number of nodes varied from 9 584 to 236 206 (Fig. 3).

It is seen from Fig. 3 that the computational Nu_{av} of each tube becomes independent from the mesh for the mesh of about 63 824 nodes. Hence, the mesh of 63 824 nodes is considered here-onwards to optimize the time and the accuracy of the solution.

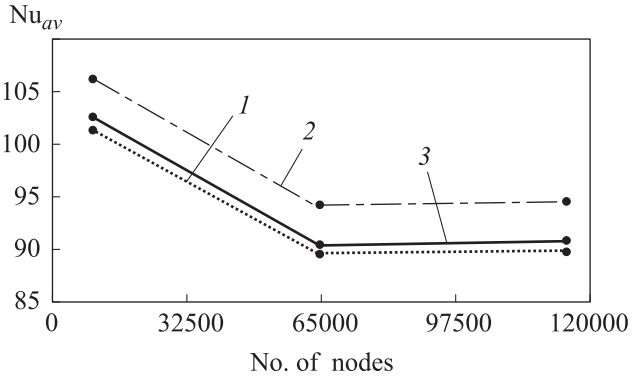

Fig. 3. Mesh-sensitivity analysis at u = 12 m/s for cam-shaped (*1*); drop-shaped tube (*2*), circular (*3*)

Discussion of the results obtained. *Numerical results verification.* In order to validate the numerical model, the numerical results of the present study were validated with the corresponding experimental one [2, 6, 9] of Nu_{av} and Euler number Eu in the same range of values of Reynolds numbers. Figure 4 shows

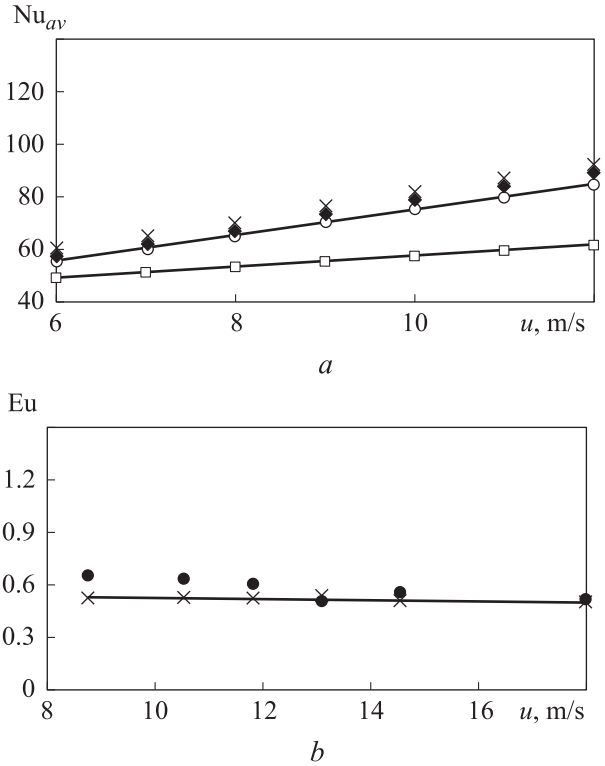

Fig. 4. Validation of Nu_{av} versus u (*a*); validation of Eu versus u (*b*):
a) o — exp. circular-shaped [2]; × — num. circular-shaped; □ — exp. cam-shaped [6]; ◆ — num. cam-shaped; *b*) × — exp. drop-shaped, D = 38 mm [9]; ● — *ANSYS*

increased turbulence which leads to the amplification of the convective heat transfer. Thus, the model and the method of the CFD simulation presented in this study is reliable.

Velocity contours. Figure 5 illustrates the velocity contours at u = 6, 12 m/s for the three studied tubes. It is noticed that the vortex area behind the tubes gradually decreases for the circular, cam, and drop-shaped tube, respectively, which affects heat transfer and fluid flow characteristics. The flow separation occurs as a result of travelling of the boundary layer far enough against an adverse pressure gradient, that makes the velocity of the particles nearest to the surface falls almost to zero. With increasing the air velocity from 6 to 12 m/s, the vortex area in wake zone surface of tubes increases (Fig. 5, *b, d, e*).

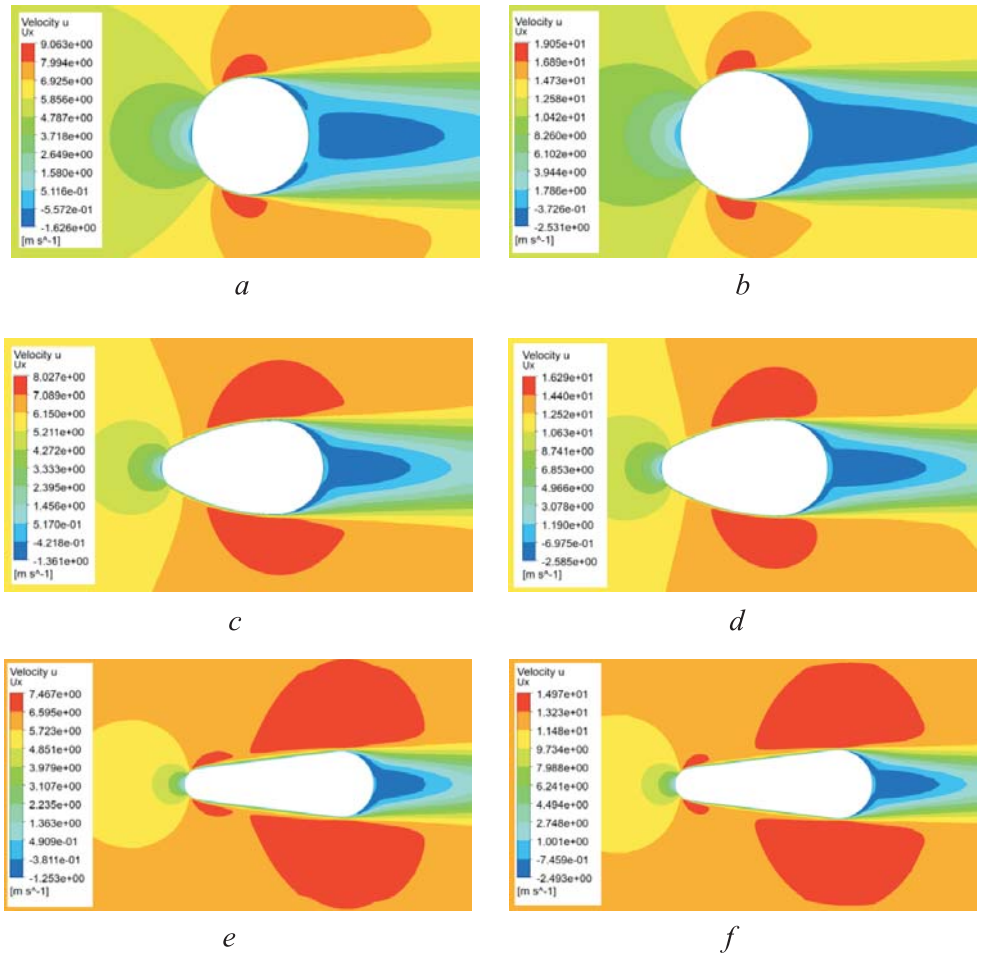

Fig. 5. Velocity contours for circular (*a, b*); cam-shaped (*c, d*); drop-shaped tube (*e, f*) at u = 6 (*a, c, e*), 12 m/s (*b, d, f*)

Heat transfer characteristics. Figure 6 demonstrates contours of static temperature for different shapes of the tube for selected velocities. The temperature of the air increases by gaining the heat from the tube surface. The maximum temperature of 82.85 °C is observed at the surface of the tubes (boundary condition). It is seen that at u = 6 m/s, the thermal boundary layer is thicker than that for u = 12 m/s. This is attributed to the separation of the flow over the tube surfaces, which contributes to a further improvement in heat transfer with increasing the velocity.

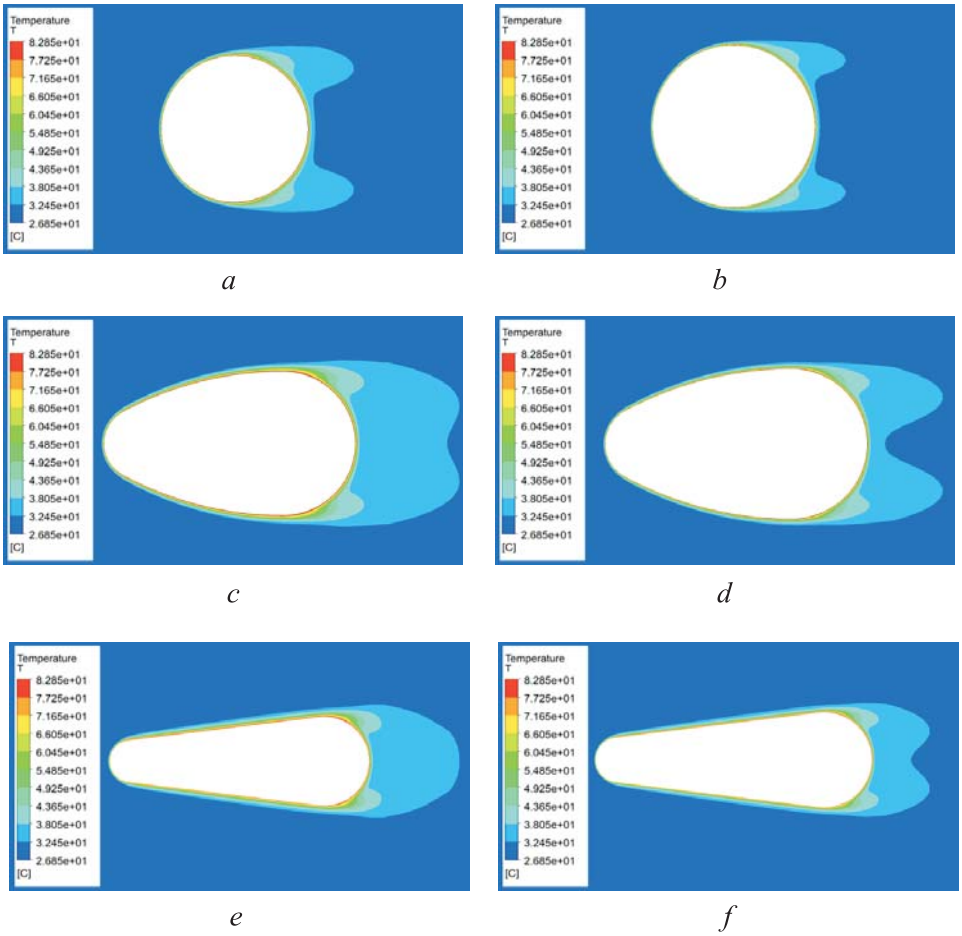

Fig. 6. Temperature contours for circular (*a, b*); cam-shaped (*c, d*); drop-shaped tube (*e, f*) at u = 6 (*a, c, e*), 12 m/s (*b, d, f*)

The local heat transfer is affected by the thickness of the boundary layer over the surface of the tube. Since the distribution of a local heat transfer coefficient α over the tube is symmetrical, the distribution of α over a half surface of each tube at u = 9 m/s given in Fig. 7 *a*. For all tubes, the local heat transfer

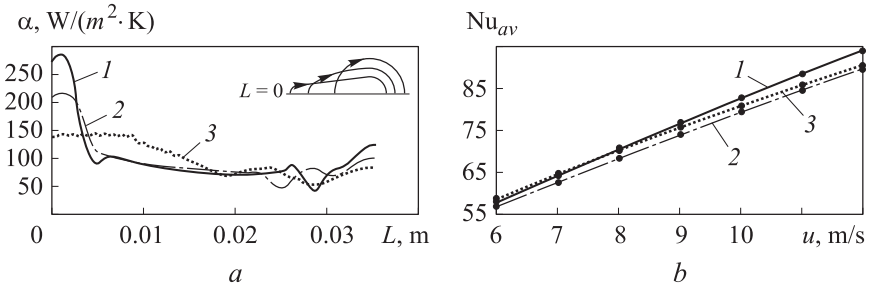

Fig. 7. The distribution of the local heat transfer coefficient (*a*); variation of average Nusselt number vs velocity (*b*) at drop-shaped tube (*1*), cam-shaped (*2*); circular (*3*)

coefficients have a maximum value at the forward stagnation point and then they decrease until reach the separation point of the boundary layer. The minimum value in Fig. 7 *a* indicates the separation point of the curves, and then the heat transfer coefficient increases again due to the occurrence of the vortex.

Figure 7 *b* shows the variations of the average Nusselt number Nu_{av} over the whole surface of each tube for the air velocity in ranger of 6–12 m/s. The average Nusselt number increases with the increase in the air velocity. At low air velocities, the difference between the average Nusselt number values for all tubes is small. It is seen that the drop-shaped tube has the best heat transfer performance compared to circular, and cam-shaped tubes. At u = 12 m/s, the maximum value of Nu_{av} for cam, circular, and drop-shaped tubes is found to be 89.73, 90.46, and 94.11, respectively.

The average Nusselt number of a tube was determined from the computational experiment results as:

$$\mathrm{Nu}_{av} = \frac{\overline{\alpha} D_{eq}}{\lambda},$$

where $\overline{\alpha} = \frac{1}{F}\int_0^F \alpha dF$ is the heat transfer coefficient averaged over whole surface of tube.

Correlation for the average non-dimensional Nusselt number for different shapes of tube based on the computational experiment was predicted by equation:

$$\mathrm{Nu}_{av} = A\,\mathrm{Re}^B\,\mathrm{Pr}^C. \qquad (1)$$

Here the thermo-physical properties [20] are calculated for the average temperature of the incoming flow. The coefficients A, B and C for Eq. (1) were computed in *Mathcad* package using least square technique (Table 1). The obtained equation is applicable for $\mathrm{Re}_{D\max} = (8.1–19.2) \cdot 10^3$ and for Prandtl number $\mathrm{Pr} \cong 0.7$.

Table 1

Coefficients *A*, *B*, *C* for the proposed correlation for $\overline{\mathrm{Nu}}$, Eq. (1)

Tube	*A*	*B*	*C*
Cam-shaped	0.1745	0.6512	0.37
Drop-shaped	0.1163	0.7028	

Pressure and friction coefficients over a tube surface. Figure 8 presents the static pressure contour for two cases of the air velocity. For all studied cases, it is clear that the pressure has the highest value at the stagnation point on the front of the tube, this is due to the fact that the flow velocity at this point tends to zero (see Fig. 5). As flow passes over the surface of the tube, the pressure decreases to the lowest value on the lateral surface. It can be seen that the drop and the cam-shaped tubes reduce pressure drop more than the circular tube. This is because they have a smaller wake zone as compared to the circular one.

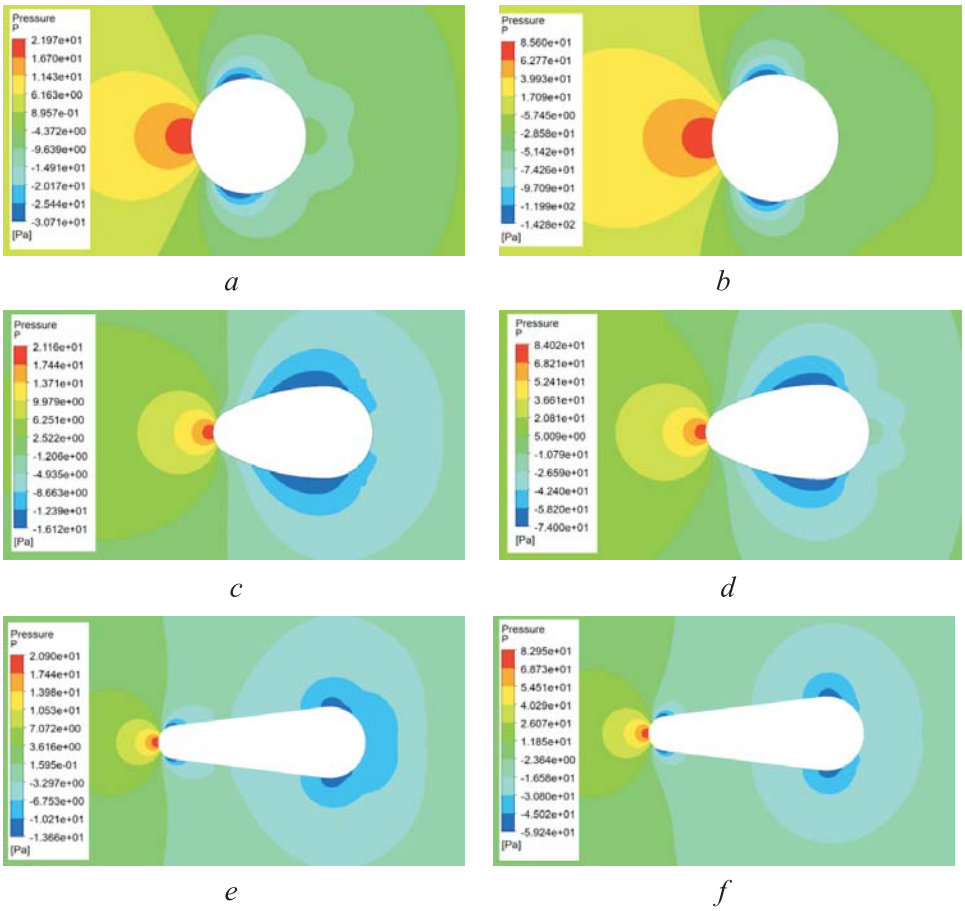

Fig. 8. Pressure contours for circular (*a, b*); cam-shaped (*c, d*); drop-shaped tube (*e, f*) at $u = 6$ (*a, c, e*), 12 m/s (*b, d, f*)

The pressure over the tube surface could be expressed through a pressure coefficient as:

$$C_{p,i} = \frac{p_i - p_\infty}{(1/2)\rho U_\infty^2},$$

where p_i is the local static pressure; p_∞ and U_∞ are the pressure and velocity of the air free stream respectively.

Figure 9 *a* shows the distribution of pressure coefficient over a half surface of the tube for u = 9 m/s. At the forward stagnation point, it is clear that all tubes have the maximum value of the pressure coefficient, which is about 1.1. At the frontal section, the drop shaped tube has a sharper drop pressure compared to other tubes. For a circular tube, C_p decreases to reach a minimum value and then increases up to the rear stagnation point of the tube. However, in the case of cam and drop-shaped tubes, there are two minimum values of C_p. This can be attributed to the fact that the flow around cam and drop-shaped tubes are similar to the flow over two circular tubes as well as two tangent arcs or lines between them. These arcs and lines lead to a deceleration of the flow along the surface of the tube and, accordingly, to an increase in pressure.

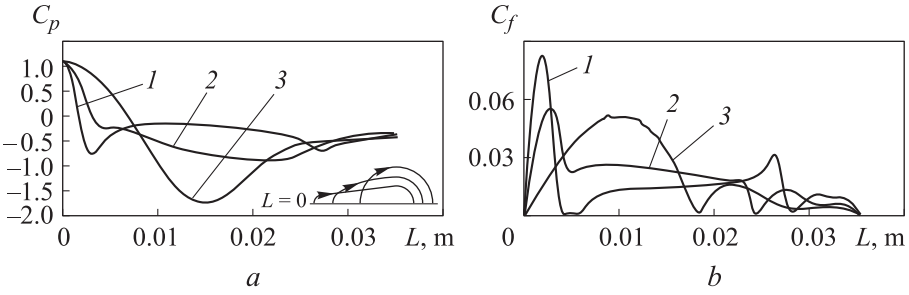

Fig. 9. Pressure coefficient distribution (*a*); skin coefficient distribution (*b*) for drop-shaped tube (*1*), cam-shaped (*2*), circular (*3*)

It should be noted that the minimum value of C_p is the point of change from a favorable to an adverse pressure gradient over the surface of the tube. Drop-shaped tube has a high favorable pressure gradient at the front of the tube and a low adverse pressure gradient on sides of the tube, which prolongs the separation of the fluid from the wall surface (see Fig. 9 *a*).

To find the location of the boundary layer separation point from the tube surface, the distributions of the skin friction coefficient C_f over a half surface of the studied tubes are plotted in Fig. 9 *b* for u = 9 m/s.

The skin friction coefficient is determined as follows:

$$C_{f,i} = \frac{\tau_{w,i}}{(1/2)\rho U_\infty^2},$$

where $\tau_{w,i}$ is a local skin shear stress on a tube surface.

The value of zero for C_f indicates that the flow is separated from the surface of the tube. For different tubes, it is seen from Fig. 9 *b* that a first zero value of C_f exists at the forward stagnation point. The location of the second zero value of the skin friction coefficient is shifted towards the rear stagnation point of the tube for a circular tube compared to a drop-shaped tube. However, it does not exist in the case of a cam-shaped tube. The highest and lowest values of C_f are observed for the drop, cam-shaped, and circular tube, respectively.

The pressure drop across the channel is represented by friction factor, as defined by [21]:

$$f = \frac{\Delta p}{\frac{l}{D_{eq}} \frac{\rho U_{\max}^2}{2}},$$

where l is a major axis of the tube; Δp is pressure drop across the test section (from the simulation results).

Figure 10 presents the friction factor for different shapes of tube. As the air velocity increases, for all cases, the friction factor for the fluid decreases. This is usually due to the fact that the overall drag consists of two combined parts: the friction drag, and the pressure drag. The friction drag is more dominant than the pressure drag at the lower velocities, which results in a higher pressure drop while the opposite occurs at the higher velocities. In the case of high velocities, the influence of viscous forces decreases while that of the inertial forc-

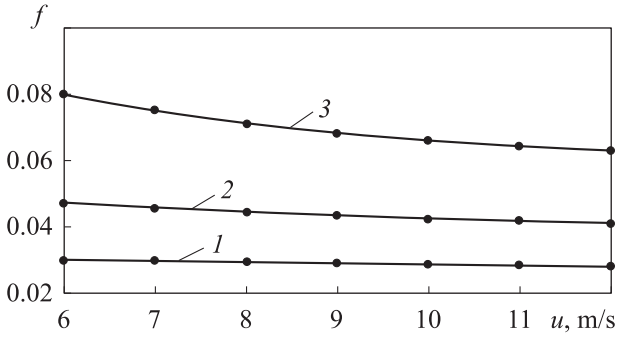

Fig. 10. Friction factor vs air velocity for drop-shaped tube (*1*), cam-shaped (*2*), circular (*3*)

es increases. Since the airflow tends to shift more turbulent, the separation point travels farther downstream, nd consequently the size of the wake and the magnitude of the pressure drag decreases. Results show that the cam and drop-shaped tubes have less friction factor compared to circular tube. Friction factor of a drop-shaped tube is about 124.66–167.91 % and 46.44–57.8 %, respectively, lower than the circular and cam-shaped tubes.

The correlations for friction factor for Reynolds number in the range of $(8.1–19.2) \cdot 10^3$ is obtained by equation:

$$f = a\mathrm{Re}^{-b}, \tag{2}$$

where *a, b* are constants, determined from the *ANSYS* data (Table 2).

Table 2

Coefficients *a, b* for the proposed Eq. (2)

Tube	*a*	*b*
Cam-shaped	0.2758	0.1946
Drop-shaped	0.0667	0.0884

Thermal-hydraulic performance. The above sections have discussed the heat transfer characteristics and the friction factor for the three shapes of tube. However, it is necessary to evaluate the combined effect of heat transfer along with friction factor associated with the flow over the tubes.

The thermal-hydraulic performance shaped tube base on a circular tube is proposed by Webb [22] as:

$$\eta = \frac{\overline{\mathrm{Nu}}_{av,cam(drop)} / \overline{\mathrm{Nu}}_{av,circ}}{f_{cam(drop)} / f_{circ}}.$$

The thermal-hydraulic performance for the entire range of the air velocity is depicted in Fig. 11. Results show that the performance of drop and cam-

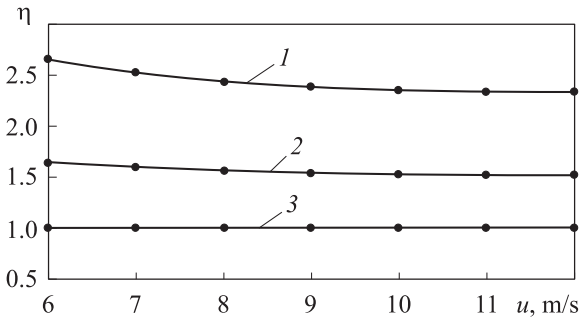

Fig. 11. Thermal-hydraulic performance of various tubes for drop-shaped tube (*1*), cam-shaped (*2*), circular (*3*)

shaped tubes is about 2.5 and 1.5 times, respectively, higher than the circular one. This can be attributed to the aerodynamic shape and lower friction factor of the drop and cam-shaped tubes compare to a circular tube. Therefore, it is clear that the drop and cam-shaped tubes perform better.

Conclusion. Numerical investigation is carried out to compare heat transfer and hydrodynamic characteristics of single circular, cam, and drop-shaped tube in cross flow. The study is performed for the Reynolds number range from $8.1 \cdot 10^3$ to $19.2 \cdot 10^3$. The main conclusions are as follows:

at the tube downstream, the drop and cam-shaped tubes have less vortex area compared to the circular one;

local heat transfer coefficients of the cam and drop-shaped tubes is significantly different from that of the circular tube. For all tubes, the local heat transfer coefficients have a maximum value at the forward stagnation point;

the highest and lowest values of C_f were occurred for the drop, cam-shaped, and circular tube, respectively;

for different shapes of tube, the results indicated that the average Nusselt number Nu_{av} increases with increasing the air velocity. In the contrary, friction factor f decreases as the air velocity increases;

friction factor of a drop-shaped tube is about 2.25–2.68 and 1.46–1.58 times, respectively, lower than the circular and cam-shaped tubes;

correlations were developed from the computational results for the studied tubes to give Nu_{av} and f in terms of Re;

thermal-hydraulic performance of drop and cam-shaped tubes is about 2.5 and 1.5 times, respectively, higher than the circular one.

The results obtained will serve as a base for further studies of the heat transfer and hydrodynamic characteristics of drop-shaped tubes bundle.

REFERENCES

[1] Žukauskas A., Ulinskas R.V. Efficiency parameters of heat transfer in tube banks. *Heat Transf. Eng.*, 1985, vol. 6, iss. 1, pp. 19–25.
DOI: https://doi.org/10.1080/01457638508939614

[2] Žukauskas A. Heat transfer from tubes in cross-flow. *Adv. Heat Transf.*, 1972, vol. 8, pp. 93–160. DOI: https://doi.org/10.1016/S0065-2717(08)70038-8

[3] Mittal S., Kumar V., Raghuvanshi A. Unsteady incompressible flows past two cylinders in tandem and staggered arrangements. *Int. J. Numer. Methods Fluids*, 1997, vol. 25, iss. 11, pp. 1315–1344. DOI: https://doi.org/10.1002/(SICI)1097-0363(19971215)25:11%3C1315::AID-FLD617%3E3.0.CO;2-P

[4] Roychowdhury G.D., Sarit K.D., Sundararajan T. Numerical simulation of laminar flow and heat transfer over banks of staggered cylinders. *Int. J. Numer. Methods Fluids*, 2002, vol. 39, iss. 1, pp. 23–40. DOI: https://doi.org/10.1002/fld.260

[5] Nishiyama H., Ota T., Matsuno T. Heat transfer and flow around elliptic cylinders in tandem arrangement. *JASME Int. J. Ser. II*, 1988, vol. 31, iss. 3, pp. 410–419.
DOI: https://doi.org/10.1299/jsmeb1988.31.3_410

[6] Lavasani A.M., Bayat H., Maarefdoost T. Experimental study of convective heat transfer from in-line cam shaped tube bank in crossflow. *Appl. Therm. Eng.*, 2014, vol. 65, iss. 1-2, pp. 85–93. DOI: https://doi.org/10.1016/j.applthermaleng.2013.12.078

[7] Merker G.P., Hanke H. Heat transfer and pressure drop on the shell-side of tube-banks having oval-shaped tubes. *Int. J. Heat Mass Transfer*, 1986, vol. 29, iss. 12, pp. 1903–1909. DOI: https://doi.org/10.1016/0017-9310(86)90008-6

[8] Horvat A., Leskovar M., Mavko B. Comparison of heat transfer conditions in tube bundle cross-flow for different tube shapes. *Int. J. Heat Mass Transfer*, 2006, vol. 49, iss. 5-6, pp. 1027–1038. DOI: https://doi.org/10.1016/j.ijheatmasstransfer.2005.09.030

[9] Terekh A.M., Rudenko A.I., Zhukova Yu.V. Aerodynamic drag and visualization of the flow around single tubes of a drop-shaped form. *Eng. Phys. Thermophy*., 2013, vol. 86, no. 2, pp. 378–384. DOI: https://doi.org/10.1007/s10891-013-0844-9

[10] Sayed Ahmed S.A.E., Ibrahiem E.Z., Mesalhy O.M., et al. Heat transfer characteristics of staggered wing-shaped tubes bundle at different angles of attack. *Heat Mass Transfer*, 2014, vol. 50, no. 8, pp. 1091–1102.
DOI: https://doi.org/10.1007/s00231-014-1323-3

[11] Sayed Ahmed S.A.E., Ibrahiem E.Z., Mesalhy O.M., et al. Effect of attack and cone angels on air flow characteristics for staggered wing-shaped tubes bundle. *Heat Mass Transfer*, 2015, vol. 51, no. 7, pp. 1001–1016.
DOI: https://doi.org/10.1007/s00231-014-1473-3

[12] Deeb R., Sidenkov D.V. Investigation of flow characteristics for drop-shaped tubes bundle using ansys package. *2020 V Int. Conf. Inform. Tech. Eng. Education (Inforino)*, Moscow, Russia, 2020, pp. 1–5.
DOI: https://doi.org/10.1109/Inforino48376.2020.9111775

[13] Deeb R., Sidenkov D.V. Numerical simulation of the heat transfer of staggered drop-shaped tubes bundle. *J. Phys.: Conf. Ser*., 2019, vol. 1359, art. 012135.
DOI: https://doi.org/10.1088/1742-6596/1359/1/012135

[14] Jafari H.H., Dehkordi B.G. Numerical prediction of fluid-elastic instability in normal triangular tube bundles with multiple flexible circular cylinders. *J. Fluids Eng.*, 2013, vol. 135, iss. 3, art. 031102.

[15] Priyank D.P., Karnav N.S., Kush V.M., et al. CFD analysis of heat exchanger over a staggered tube bank for different angle arrangement of tube bundles. *IJERT*, 2013, vol. 2, iss. 1, art. IJERTV2IS1445.

[16] Orszag S.A., Yakhot V., Flannery W.S., et al. Renormalization group modeling and turbulence simulations. *Int. Conf. Near-Wall Turbulent Flows*. Arizona, Tempe, 1993, pp. 1031–1046.

[17] Frank K. Principles of heat transfer. Stamford, Cengage Learning, 2011.

[18] Soe T.M., Khaing S.Y. Comparison of turbulence models for computational fluid dynamics simulation of wind flow on cluster of buildings in mandalay. *IJERT*, 2017, vol. 7, iss. 8, pp. 337–350.
Available at: http://www.ijsrp.org/research-paper-0817.php?rp=P686711

[19] ANSYS FLUENT reference guide. Release 16.0. ANSYS, 2015.

[20] Tsvetkov F.F., Kerimov R.V., Velichko V.I. Zadachnik po teplomassoobmenu [Heat and mass transfer problem book]. Moscow, MPEI Publ., 2008.

[21] Promvonge P., Eiamsa-ard A.S. Heat transfer enhancement in a tube with combined conical-nozzle inserts and swirl generator. *Energy Convers. Manage.*, 2006, vol. 47, iss. 18-19, pp. 2867–2882. DOI: https://doi.org/10.1016/j.enconman.2006.03.034

[22] Webb R.L. Performance evaluation criteria for use of enhanced heat transfer surfaces in heat exchanger design. *Int. J. Heat Mass Transfer*, 1981, vol. 24, iss. 4, pp. 715–726. DOI: https://doi.org/10.1016/0017-9310(81)90015-6

Deeb Rawad — Post-Graduate Student, Assistant, Department of Theoretical Bases of Heat Engineering, National Research University Moscow Power Engineering Institute (Krasnokazarmennaya ul. 14, Moscow, 111250 Russian Federation).

Sidenkov D.V. — Cand. Sc. (Eng.), Assist. Professor, Department of Theoretical Bases of Heat Engineering, National Research University Moscow Power Engineering Institute (Krasnokazarmennaya ul. 14, Moscow, 111250 Russian Federation).

Salokhin V.I. — Cand. Sc. (Eng.), Head of Mechanics Department, Russian Institute for Scientific and Technical Information (Usievicha ul. 20, Moscow, 125190 Russian Federation).

Please cite this article as:

Deeb R., Sidenkov D.V., Salokhin V.I. Numerical investigation of thermal-hydraulic performance of circular and non-circular tubes in cross-flow. *Herald of the Bauman Moscow State Technical University, Series Natural Sciences*, 2021, no. 2 (95), pp. 102–117. DOI: https://doi.org/10.18698/1812-3368-2021-2-102-117